




Article

# Cavity Closure of 2-Hydroxypropyl- $\beta$ -Cyclodextrin: Replica Exchange Molecular Dynamics Simulations

Khanittha Kerdpol <sup>1</sup>, Jintawee Kicuntod <sup>2</sup>, Peter Wolschann <sup>2,3,4</sup>, Seiji Mori <sup>5</sup>,  
Chompoonut Rungnim <sup>6</sup> , Manaschai Kunaseth <sup>6</sup> , Hisashi Okumura <sup>7</sup>,  
Nawee Kungwan <sup>1,8,\*</sup>  and Thanyada Rungrotmongkol <sup>2,9,10,\*</sup>

<sup>1</sup> Department of Chemistry, Faculty of Science, Chiang Mai University, Chiang Mai 50200, Thailand; khanittha.view@gmail.com

<sup>2</sup> Structural and Computational Biology Research Unit, Department of Biochemistry, Faculty of Science, Chulalongkorn University, Bangkok 10330, Thailand; jintawee.ki@gmail.com (J.K.); karl.peter.wolschann@univie.ac.at (P.W.)

<sup>3</sup> Department of Pharmaceutical Chemistry, University of Vienna, Vienna 1090, Austria

<sup>4</sup> Institute of Theoretical Chemistry, University of Vienna, Vienna 1090, Austria

<sup>5</sup> Institute of Quantum Beam Science, Graduate School of Science and Engineering, Ibaraki University, 2-1-1 Bunkyo, Mito, Ibaraki 310-8512, Japan; seiji.mori.compchem@vc.ibaraki.ac.jp

<sup>6</sup> National Nanotechnology Center (NANOTEC), National Science and Technology Development Agency (NSTDA), Pathum Thani 12120, Thailand; chompoonut@nanotec.or.th (C.R.); manaschai@nanotec.or.th (M.K.)

<sup>7</sup> Research Center for Computational Science, Institute for Molecular Science, Okazaki, Aichi 444-8585, Japan; hokumura@ims.ac.jp

<sup>8</sup> Center of Excellence in Materials Science and Technology, Chiang Mai University, Chiang Mai 50200, Thailand

<sup>9</sup> Ph.D. Program in Bioinformatics and Computational Biology, Faculty of Science, Chulalongkorn University, Bangkok 10330, Thailand

<sup>10</sup> Molecular Sensory Science Center, Faculty of Science, Chulalongkorn University, 254 Phayathai Road, Patumwan, Bangkok 10330, Thailand

\* Correspondence: naweekung@gmail.com (N.K.); thanyada.r@chula.ac.th (T.R.); Tel.: +66-5394-3341 (ext. 101) (N.K.); +66-2218-5426 (T.R.)

Received: 13 December 2018; Accepted: 11 January 2019; Published: 16 January 2019



**Abstract:** 2-Hydroxypropyl- $\beta$ -cyclodextrin (HP $\beta$ CD) has unique properties to enhance the stability and the solubility of low water-soluble compounds by inclusion complexation. An understanding of the structural properties of HP $\beta$ CD and its derivatives, based on the number of 2-hydroxypropyl (HP) substituents at the  $\alpha$ -D-glucopyranose subunits is rather important. In this work, replica exchange molecular dynamics simulations were performed to investigate the conformational changes of single- and double-sided HP-substitution, called 6-HP $\beta$ CDs and 2,6-HP $\beta$ CDs, respectively. The results show that the glucose subunits in both 6-HP $\beta$ CDs and 2,6-HP $\beta$ CDs have a lower chance of flipping than in  $\beta$ CD. Also, HP groups occasionally block the hydrophobic cavity of HP $\beta$ CDs, thus hindering drug inclusion. We found that HP $\beta$ CDs with a high number of HP-substitutions are more likely to be blocked, while HP $\beta$ CDs with double-sided HP-substitutions have an even higher probability of being blocked. Overall, 6-HP $\beta$ CDs with three and four HP-substitutions are highlighted as the most suitable structures for guest encapsulation, based on our conformational analyses, such as structural distortion, the radius of gyration, circularity, and cavity self-closure of the HP $\beta$ CDs.

**Keywords:** 2-hydroxypropyl- $\beta$ -cyclodextrin (HP $\beta$ CD); replica exchange molecular dynamics (REMD); conformational change; cavity self-closure

## 1. Introduction

Cyclodextrins (CDs) are cyclic oligosaccharides, which received much attention in various technical applications, due to their unique properties. In the pharmaceutical industry, they are widely used to improve the stability and the solubility of insoluble drugs in water or organic solvent–water mixtures by molecular encapsulation [1–9]. The ability of the encapsulation of CDs with drugs strongly depends on the structural nature of the applied CDs. There are several different kinds of CDs that are defined by number of glucose units, and the most common CDs are  $\alpha$ -,  $\beta$ -, and  $\gamma$ -CD, with different number of  $\alpha$ -D-glucopyranose units ( $\alpha = 6$ ,  $\beta = 7$  and  $\gamma = 8$ ). Among these CDs, a derivative of  $\beta$ -cyclodextrin ( $\beta$ CD) named as 2-hydroxypropyl- $\beta$ -cyclodextrin (HP $\beta$ CD), shown in Figure 1, has been found to be more soluble and to have a lower toxicity than  $\beta$ CD [10–13].

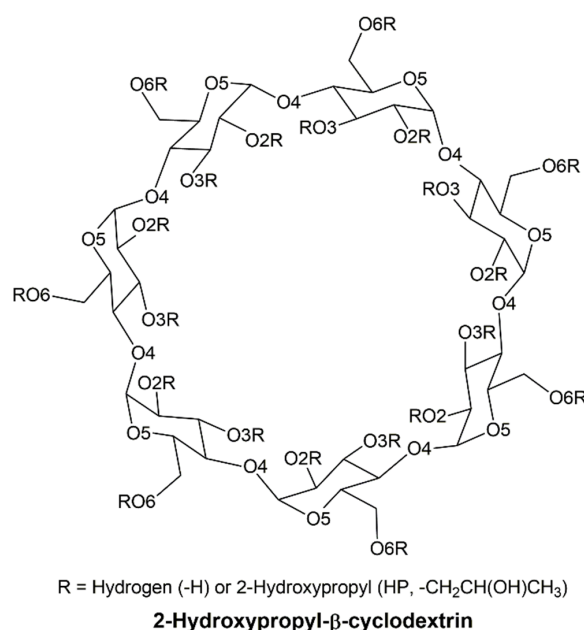


**Figure 1.** Schematic representation of 2-hydroxypropyl- $\beta$ -cyclodextrin (HP $\beta$ CD), which comprises seven glucopyranose units.

HP $\beta$ CD, a partially substituted poly(hydroxypropyl) ether of  $\beta$ CD, is commercially available as a mixture with a certain range of degrees of substitution [11,13–16]. The separation of the individual derivatives and isomers from each other is rather difficult, in particular, at the industrial scale. Also, a selective synthesis of the individual isomer is not easy; therefore, a characterization of various derivatives with regard to their inclusion ability is not possible. However, theoretical studies, particularly molecular dynamics simulations, have become a popular tool for providing this important information. By investigating the molecular structural behavior at the atomistic level of each substituted derivative, compounds with a certain degree of substitution of HP $\beta$ CD can be evaluated. Note that in the technical product, the degree of substitution exists randomly, with different numbers of HP at other positions (e.g., at different glucose units at the 2, 3, and 6 positions), which depends on the concentration of the alkaline solution during the synthesis. Normally,  $\beta$ CD alkylations are observed at the O2 and O6 positions [13,17,18]. Therefore, HP $\beta$ CD with substitutions at O2 (the most acidic position) and O6 (the most accessible position) with different degrees of substitution have been intensively investigated [11,13–16,19–22].

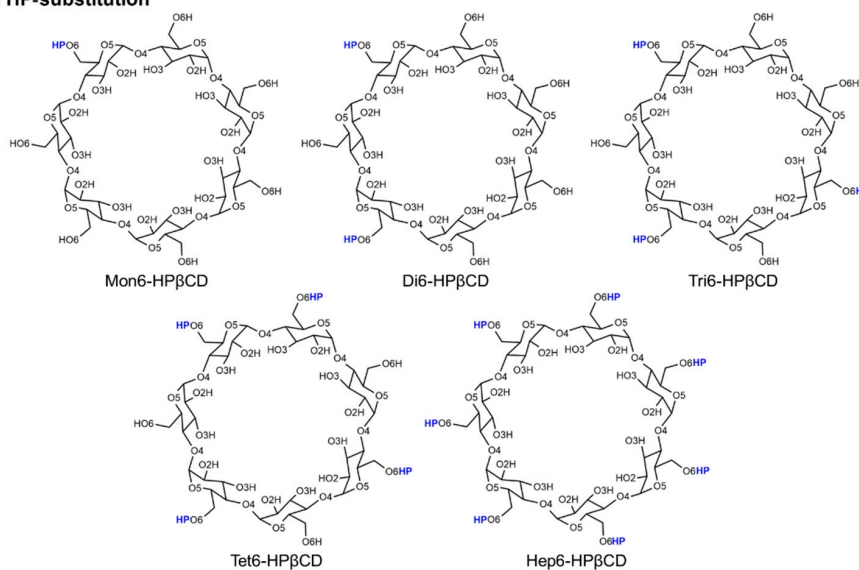
Generally, it is difficult to explore the conformations of biomolecules with complicated free energy surfaces and a larger number of local minima by single conventional simulation at a low temperature condition. To overcome this problem, the replica-exchange molecular dynamics simulations (REMD) [23,24], which is one of the most effective methods with generalized-ensemble algorithms, is applied by non-interacting replica exchange at various temperatures [23–27]. This could

allow us to obtain the information of the temperature dependence. In the present study, we applied the REMD method on  $\beta$ CD and HP $\beta$ CDs models to study the conformational change affected by the different numbers of HP-substitutions on the O2 and/or O6 atoms. The structural behaviors of all models were analyzed based on structural distortion analysis, the radius of gyration, circularity, and the cavity self-closure of the HP $\beta$ CDs. By doing so, the best candidate of the HP $\beta$ CDs with a suitable amount of HP-substitution, representing the perfect conical shape for molecular encapsulation, will be provided as a useful guideline for the suitable substitution degree of HP $\beta$ CD.

## 2. Computational Methods

The optimized structures of native  $\beta$ CD and Hep6-HP $\beta$ CD were taken from our previous studies [28,29]. The other HP $\beta$ CD derivatives were prepared by different numbers of 2-hydroxypropyl (HP) substitutions at the O2 or O6 positions on  $\alpha$ -D-glucopyranose units with substitution degrees of around 0.14–1.14 from one to eight HP-substitutions on  $\beta$ CD, as shown in Figure 2. The HP-substitutions on  $\beta$ CD in this work were divided into two groups, single- and double-sided substitutions. For the single-sided HP-substitution (Figure 2a), the HP groups were substituted with from one up to seven HP, only on O6 atoms of the primary rim (called as 6-HP $\beta$ CDs), because the O6 is more reactive compared to O2 atoms of the secondary rim. In the case of double-sided HP-substitution (Figure 2b), the structures were generated by introducing from one up to four HP groups at the O2 atoms of the non-substituted glucose units (called as 2,6-HP $\beta$ CD), as defined in Table 1.

### (a) Single-sided HP-substitution



### (b) Double-sided HP-substitution

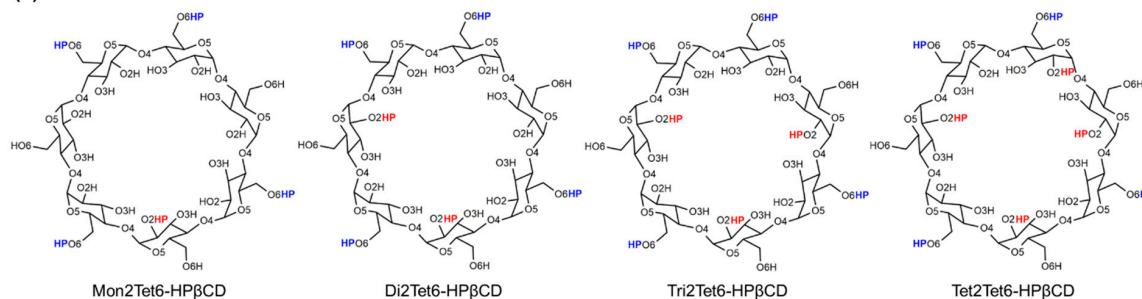


**Figure 2.** Models introducing 2-hydroxypropyl (HP) groups at the O2 (red) and/or O6 (blue) positions on glucose subunits.

**Table 1.** Model summary of introducing HP groups at the O2 and/or O6 positions on glucose subunits.

Models	Degree of Substitution	O2 Substitution	O6 Substitution
$\beta$ CD	0.00	None	None
<b>Single-sided HP-substitution</b>			
Mon6-HP $\beta$ CD	0.14	None	1 (At glucose unit 1)
Di6-HP $\beta$ CD	0.28	None	2 (At glucose units 1 and 3)
Tri6-HP $\beta$ CD	0.43	None	3 (At glucose units 1, 3, and 5)
Tet6-HP $\beta$ CD	0.57	None	4 (At glucose units 1, 3, 5, and 7)
Hep6-HP $\beta$ CD	1.00	None	7 (At all glucose units)
<b>Double-sided HP-substitution</b>			
Mon2Tet6-HP $\beta$ CD	0.71	1 (At glucose unit 4)	4 (At glucose units 1, 3, 5, and 7)
Di2Tet6-HP $\beta$ CD	0.85	2 (At glucose units 2 and 6)	4 (At glucose units 1, 3, 5, and 7)
Tri2Tet6-HP $\beta$ CD	1.00	3 (At glucose units 2, 4, and 6)	4 (At glucose units 1, 3, 5, and 7)
Tet2Tet6-HP $\beta$ CD	1.14	4 (At glucose units 2, 4, 6, and 7)	4 (At glucose units 1, 3, 5, and 7)

Overall, 10 CD structures were generated, to study how different numbers of HP influence the structural behavior, using REMD simulations. A detailed information of the REMD method is given elsewhere [23,24]. The REMD simulations were performed by the Amber 14 package [30]. The parameters of  $\beta$ CD and HP $\beta$ CDs were taken from the Glycam06 carbohydrate force field [31,32], with the solvation model based on the generalized Born (GB) implicit solvent model, Igb5, which gives a suitable description of cyclodextrin  $\epsilon$ CD, as reported by Khuntawee et al. [33], and the smaller sizes of CDs ( $\alpha$ CD- $\delta$ CD, unpublished data) relative to the available crystal structures and MD studies in the explicit solvent model. The initial structures of  $\beta$ CD and all HP $\beta$ CDs were fully minimized with 2000 steps of the steepest descent method, followed by 1000 steps of the conjugated gradient method to relax the structures before simulation. The REMD simulations were performed for 30 ns per replica, including an equilibration step for 5 ns, and the conformations at all temperatures were collected every 1 ps for 25 ns. The temperature distribution and the number of replicas were tested to obtain a reasonable replica exchange simulation. The overlapping between the potential energy distributions of eight replicas is shown in Figure S1 of the Supplementary Materials. The results confirm that the temperature from 269.5 K to 570.9 K, with interval steps of around 30–60 K, was proper for the present case.

The structural distortions of all HP $\beta$ CDs were analyzed by distances analysis, as defined in Figure 3. Firstly, the distances of adjacent glucopyranose units,  $d_{1(i)}[\text{O}2_{(i)}\text{--O}3_{(i+1)}]$  was defined as the distance between the secondary hydroxyl groups related to the intramolecular hydrogen bonds of the wider CD rim, as labeled in Figure 3a. Secondly, the distance between the glycosidic oxygen atoms,  $d_{2(i)}[\text{O}4_{(i)}\text{--O}4_{(i+1)}]$  is calculated for monitoring the ellipticity of the CDs. The probability distributions of the  $d_{1(i)}$  and  $d_{2(i)}$  were calculated using Equation (1) in terms of free energy:

$$F(x, y) = -k_B T \log[P(x, y)] \quad (1)$$

where  $k_B$  is the Boltzmann constant,  $T$  is the absolute temperature, and  $P(x, y)$  is the probability of  $x$  for  $d_{1(i)}[\text{O}2_{(i)}\text{--O}3_{(i+1)}]$  and  $y$  for  $d_{2(i)}[\text{O}4_{(i)}\text{--O}4_{(i+1)}]$  distances.

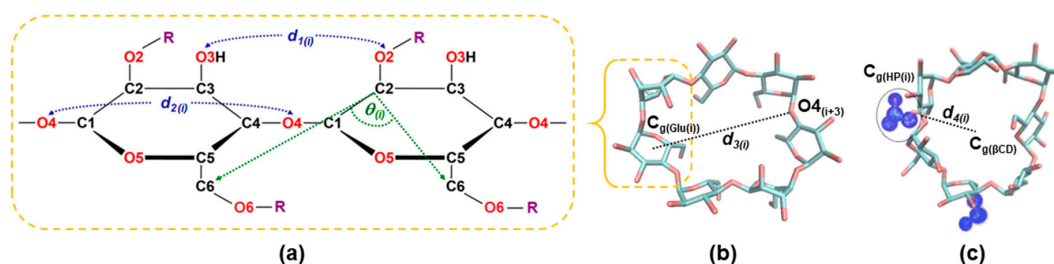


**Figure 3.** (a) Cyclodextrin (CD) fragment showing the atomic labels and important structural parameters,  $d_{1(i)}[\text{O}2_{(i)}\text{--O}3_{(i+1)}]$ ,  $d_{2(i)}[\text{O}4_{(i)}\text{--O}4_{(i+1)}]$ , and  $\theta_{(i)}[\text{C}6_{(i)}\text{--C}2_{(i+1)}\text{--C}6_{(i+1)}]$ . (b) Set of diameters,  $d_{3(i)}[\text{C}_g(\text{Glu}(i))\text{--O}4_{(i+3)}]$ , for circularity. (c) Set of  $d_{4(i)}[\text{C}_g(\beta\text{CD})\text{--C}_g(\text{HP}(i))]$  for studying cavity self-closure.

Next, the flips of glucose subunits for various conformations were monitored by angle between a pair of adjacent glucose units,  $\theta_{(i)}[\text{C6}_{(i)}-\text{C2}_{(i+1)}-\text{C6}_{(i+1)}]$ , as defined in Figure 3a. Without the flipping, the C6 atoms are in the same site with the adjacent unit. Thus, the  $\theta_{(i)}[\text{C6}_{(i)}-\text{C2}_{(i+1)}-\text{C6}_{(i+1)}]$  values in no-flip structures are less than 90 degrees. In contrast, when the unit was flipped, the C6 atoms were opposite to those of the adjacent unit, and its  $\theta_{(i)}[\text{C6}_{(i)}-\text{C2}_{(i+1)}-\text{C6}_{(i+1)}]$  was higher than 90 degrees. In addition, the radius of gyration ( $R_g$ ) was calculated. The  $R_g$  represents the mass-weighted scalar length of each atom from the center of gravity of the molecule, calculated using Equation (2).

$$R_g = \sqrt{\frac{\sum_{i=1}^N m_i (r_i - r_{cm})^2}{\sum_{i=1}^N m_i}} \quad (2)$$

where  $N$  is the number of atoms,  $m_i$  is the mass of atom  $i$ ,  $r_i$  is the Cartesian position vector of atom  $i$ , and  $r_{cm}$  is the center of mass of CD.

The next parameter is a modified circularity ( $C$ ), which is a dimensionless shape factor based on our previous work [34]. Here, we measured the diameter  $d_{3(i)}[\text{C}_{g(\text{Glu}(i))}-\text{O4}_{(i+3)}]$ , which is a distance between the center of mass of the  $i$ -th glucose unit ( $\text{C}_{g(\text{Glu}(i))}$ ) and the glycosidic oxygen atom of the opposite glucose unit ( $\text{O4}_{(i+3)}$ ), as depicted in Figure 3b. There are seven  $d_{3(i)}$  parameters for each HP $\beta$ CDs snapshot, since there are seven glucose subunits in  $\beta$ CDs. Hence,  $C$  is defined as:

$$C = \frac{\min_{i \in \{1..7\}} (d_{3(i)})}{\max_{i \in \{1..7\}} (d_{3(i)})} \quad (3)$$

Note that the value of  $C$  is in a range of  $0 < C \leq 1$ . If  $C$  is equal to 1.0, where  $\min(d_{3(i)}) = \max(d_{3(i)})$ , it means that the cavity has a perfectly circular shape. However, when  $C$  becomes deviated from 1.0, this is an indication for conformational changes to an elliptical shape. Finally, in order to study the cavity self-closure of HP $\beta$ CDs, we define the  $d_{4(i)}[\text{C}_{g(\beta\text{CD})}-\text{C}_{g(\text{HP}(i))}]$  parameter, which is the distance of the center of mass between the  $\beta$ CD ring and each HP group, as demonstrated in Figure 3c. All parameters were analyzed from 25,000 snapshots taken from REMD simulations. The analyzed results at 300 K will be presented and discussed in the next section, while those of other temperatures are provided in the Supplementary Materials.

### 3. Results and Discussion

#### 3.1. Structural Analysis

##### 3.1.1. Structural Distortion of Glucose Units in the HP $\beta$ CDs

To investigate the conformational changes of  $\beta$ CD and all selected HP $\beta$ CDs, the probability distributions of  $d_{1(i)}[\text{O2}_{(i)}-\text{O3}_{(i+1)}]$  and  $d_{2(i)}[\text{O4}_{(i)}-\text{O4}_{(i+1)}]$  distances for all models at 300 K were calculated in terms of free energy, using Equation (1), and these are plotted in Figure 4a. The contour graphs give the values of the distance probability, where the denoted darkest blue color (ranked from dark red to blue) represents the lowest free energy.

In the case of  $\beta$ CD, three conformational minima (M1, M2, and M3) were detected as shown in Figure 4(a1), which is in agreement with previous results from MD in aqueous solution [29]. The most likely distribution at M1 was found with the  $d_{1(i)}$  and  $d_{2(i)}$  distances at around 3.5 and 4.5 Å, respectively, describing the almost perfect conical shape of the  $\beta$ CD ring. The second and third main populations were M2 and M3, with  $d_{1(i)}/d_{2(i)}$  of around 5.5 Å/4.5 Å and 5.0 Å/5.5 Å, respectively. When comparing  $\beta$ CD with a large-ring CD ( $\epsilon$ CD) by the REMD method [33], three important minima were found to be similar to the  $\beta$ CD results, but the M3 population of  $\epsilon$ CD was higher than that of  $\beta$ CD, due to the



large size and the high flexibility of the macroscopic ring, having a higher probability of flipping the glucopyranose units in the large-ring system.

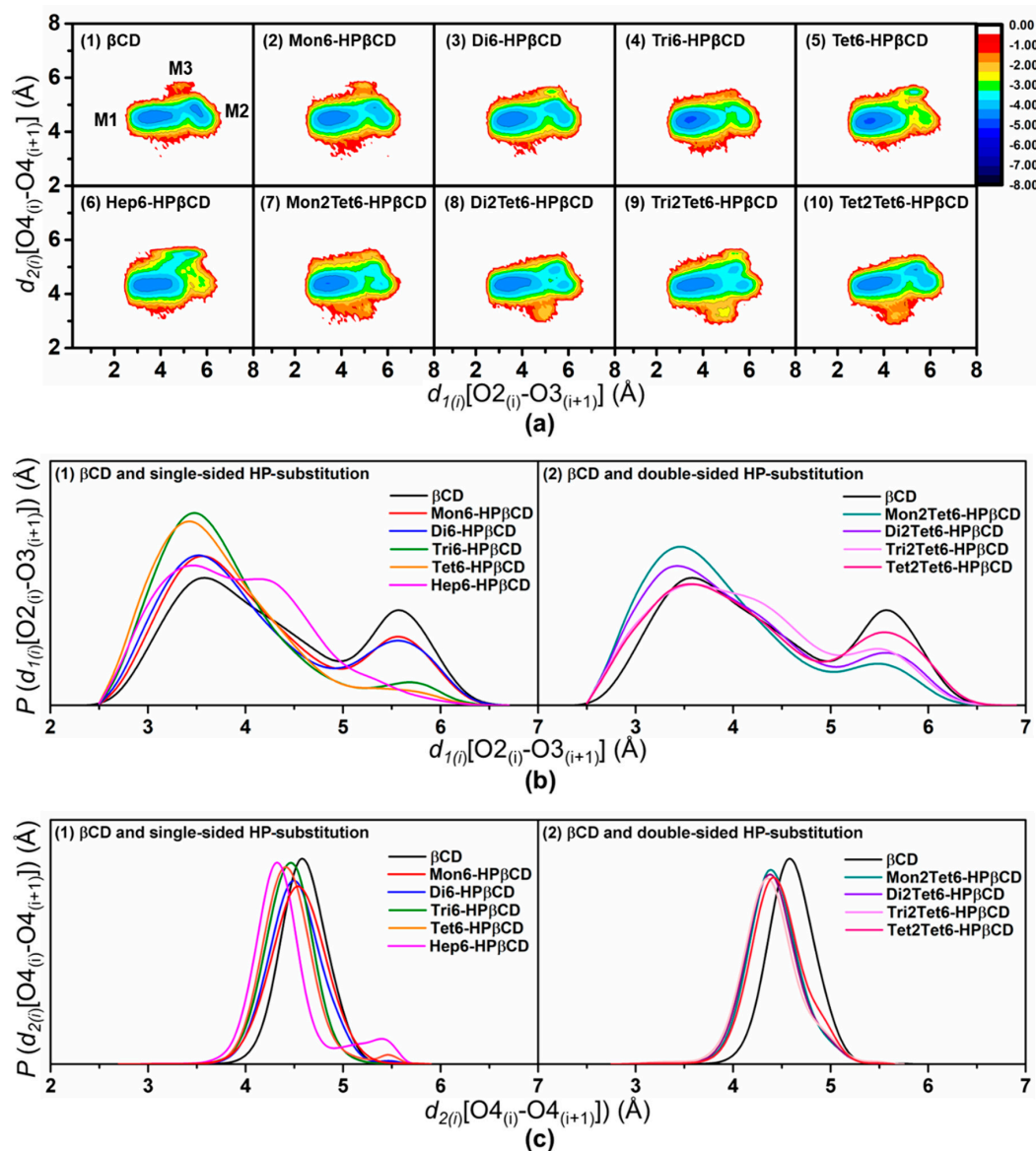


**Figure 4.** (a) Contour graphs of the probability distributions in terms of free energy, (b) the probability of  $d_{1(i)}$ , and (c) the probability of  $d_{2(i)}$  from a total of 25,000 snapshots at 300 K of REMD simulations with the glycam06 force field for  $\beta$ CD and HP $\beta$ CDs.

From all of the free energy plots of HP $\beta$ CDs with single- and double-sided HP-substitutions, the  $d_{2(i)}[O4_{(i)}-O4_{(i+1)}]$  values fluctuated in the range of 4.0–5.0 Å, implying that the backbone structures of HP $\beta$ CD were not greatly affected by the HP-substitution groups. In contrast, it was noticeable that  $d_{1(i)}[O2_{(i)}-O3_{(i+1)}]$  was in a wide range around 2.5–6.5 Å. Therefore, we plotted the probability of  $d_{1(i)}[O2_{(i)}-O3_{(i+1)}]$  and  $d_{2(i)}[O4_{(i)}-O4_{(i+1)}]$ , as depicted in Figure 4b,c, respectively, in order to compare the conformational minima among the models. For HP $\beta$ CDs with single-sided HP-substitutions, the most dominant population of  $d_{1(i)}[O2_{(i)}-O3_{(i+1)}]$  for the Tri6- and Tet6-HP $\beta$ CDs was around 3.5 Å, indicating the narrow behavior of their secondary rim. Additionally, the conformational changes of other models were quite similar to the native  $\beta$ CD, except for Hep6-HP $\beta$ CD with  $d_{1(i)}[O2_{(i)}-O3_{(i+1)}]$  at around 4.0–5.0 Å. Consequently, M3 was found in Hep6-HP $\beta$ CD higher than  $\beta$ CDs and the other 6-HP $\beta$ CDs, resulting from the steric hindrance of seven HP groups at the primary rim.

In the case of HP $\beta$ CDs with double-sided HP-substitution, the conformational changes were quite similar to the  $\beta$ CD, in which three main probability distributions were found, following this order: M1 > M2 > M3. When increasing the number of HP at the O2 positions, the M1 population decreased, while the M2 population increased, as depicted in Figure 4(a7–a10), which were related to the distribution of  $d_{1(i)}[\text{O}2_{(i)}\text{--O}3_{(i+1)}]$  (Figure 4(b2)). In addition, the new probability distribution with  $d_{1(i)}/d_{2(i)}$  around 4.3 Å/3.5 Å was observed when adding a HP group on the secondary rim, and this probability distribution was enhanced when increasing the number of HP at the O2 positions.

The results indicate that the substitution of the HP groups on narrow and/or wider rims directly affected the distortion in the  $\beta$ CD ring. It is worth noting that the M1 population was dramatically increased, whilst M2 was decreased and M3 completely disappeared due to complexation with low-water-soluble compounds [35–37].

### 3.1.2. Flipping of the HP $\beta$ CDs

It is noticeable that the flips of glucose subunits were related directly to the distortion of the CD structure. As mentioned earlier, a flip of the glucose units was counted when  $\theta_{(i)}[\text{C}6_{(i)}\text{--C}2_{(i+1)}\text{--C}6_{(i+1)}]$  was higher than 90 degrees. According to the  $\theta_{(i)}[\text{C}6_{(i)}\text{--C}2_{(i+1)}\text{--C}6_{(i+1)}]$  analysis, the results can be divided into three main different flip-conformations: which are (1) no flip; (2) one flip; (3) two flips. Example snapshots of flipped  $\beta$ CD conformations are shown in Figure 5.

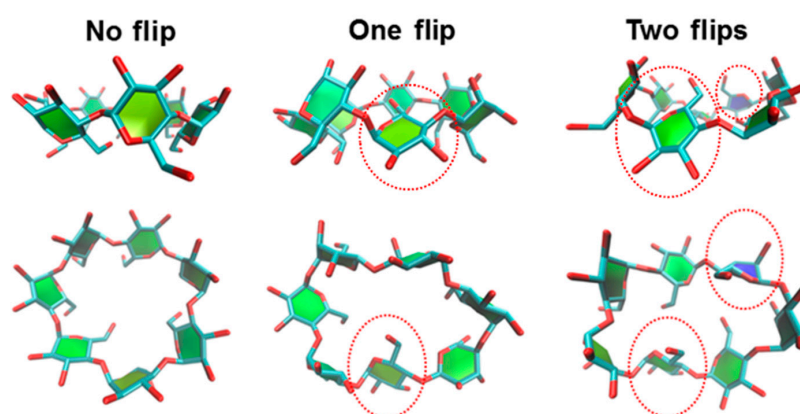


**Figure 5.** The flipped conformations of  $\beta$ CD with different numbers of flip glucose subunits, which were selected from the simulation at 300 K.

The probabilities of different numbers of flip glucose subunits for all models at 300 K are summarized in Table 2. The no-flip conformation was the main population in all models, while other higher flips (one- and two-flip) were found to be of minor importance during the simulation. In all HP $\beta$ CDs, more than 58% of no-flip conformations were observed, whereas  $\beta$ CD showed higher values of one- and two-flip conformations. The highest percentages of one- and two-flip conformations in  $\beta$ CD corresponded to the long length of  $d_{1(i)}[\text{O}2_{(i)}\text{--O}3_{(i+1)}]$  detected around 5.0–6.0 Å in the M2 population, as shown in Figure 4(a1). With an increasing number of HP only at O6 positions of glucose subunits, the no-flip population increased by up to 75–78% in Tri6- and Tet6-HP $\beta$ CDs. Meanwhile, the one-flip population decreased from 35% to 21%. These results were related to the large population of  $d_{1(i)}[\text{O}2_{(i)}\text{--O}3_{(i+1)}]$  at 3.5 Å for Tri6- and Tet6-HP $\beta$ CDs. For HP $\beta$ CDs with double-sided HP-substitution, the no-flip population also increased when compared with those of native  $\beta$ CD. However, the one- and two-flip populations of these of double-sided HP-substitutions were higher than those of Tet6-HP $\beta$ CDs. In addition, the trends of these flips were not significantly different at other temperatures, as shown in Table S1. The percentage of no-flip angles correlates with M1, which is the most populated state during simulation, and the percentages of flip angles relate with M2 and M3, in which the glucopyranose subunits flip and the intramolecular hydrogen bonds of the wider CD rim disappear. Thus, glucose subunits in both 6-HP $\beta$ CDs and 2,6-HP $\beta$ CDs have a lower chance to flip (22–31% of the flip angle)

than in  $\beta$ CD (42% of flip angle), which is in agreement with their inclusion efficiency reported in our previous study [22].

**Table 2.** The probability of different numbers of flip glucose subunits in  $\beta$ CD and HP $\beta$ CDs, using the flip angle parameter,  $\theta_{(i)}[C6_{(i)}-C2_{(i+1)}-C6_{(i+1)}]$  at 300K (criteria: values higher than 90 degrees).

Models	The Percentage of the Flip Angle (%)		
	No Flip	One Flip	Two Flips
$\beta$ CD	58	35	7
<b>Single-sided HP-substitution</b>			
Mon6-HP $\beta$ CD	69	28	3
Di6-HP $\beta$ CD	74	23	3
Tri6-HP $\beta$ CD	75	24	1
Tet6-HP $\beta$ CD	78	21	1
Hep6-HP $\beta$ CD	73	25	2
<b>Double-sided HP-substitution</b>			
Mon2Tet6-HP $\beta$ CD	77	22	1
Di2Tet6-HP $\beta$ CD	75	24	1
Tri2Tet6-HP $\beta$ CD	70	28	2
Tet2Tet6-HP $\beta$ CD	74	24	2

### 3.1.3. Radius of Gyration

The flipping of the glucose subunits directly influences the distortion of the macrocyclic ring, as shown in Figure 5 (top view of the different flipped conformations). Therefore, the shapes of all models were investigated in terms of the radius of gyration ( $R_g$ ), and the results are shown in Figure 6. The average of  $R_g$  of native  $\beta$ CD, Mon6-, Di6-, Tri6-, Tet6-, and Hep6-HP $\beta$ CDs are 6.18, 6.38, 6.39, 6.45, 6.55, and 6.85 Å, respectively, and those of Mon2Tet6-, Di2Tet6-, Tri2Tet6-, and Tet2Tet6-HP $\beta$ CDs are 6.45, 6.46, 6.65, and 6.85 Å. The results show that the average  $R_g$  trends to increase when adding more HP groups, which are similar to the  $R_g$  results from a molecular dynamics simulation, as reported by Yong et al. [17]. However, for Hep6-HP $\beta$ CD and Tri2Tet6-HP $\beta$ CD with the same degree of substitution (1.00), the average  $R_g$  of Hep6-HP $\beta$ CD was higher than that of Tri2Tet6-HP $\beta$ CD, because of the higher steric hindrance of the seven HP groups at the primary rim of Hep6-HP $\beta$ CD. Overall, the  $R_g$  in the substituted models was observed to be higher than the native  $\beta$ CD, because of the fluctuation and steric hindrance of the HP groups.

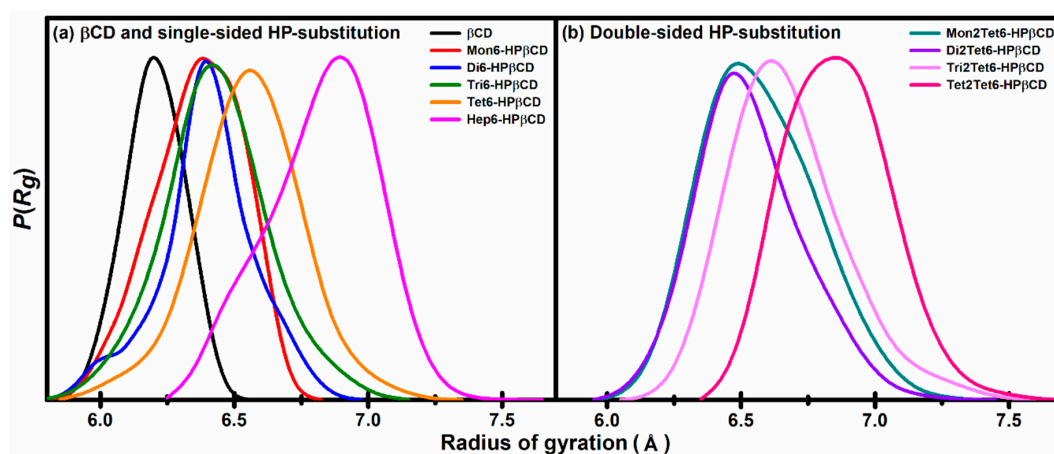


**Figure 6.** The probability of the radius of gyration for  $\beta$ CD and all HP $\beta$ CDs at 300 K.



### 3.1.4. Circularity

To determine the effect of the HP-substitutions on the geometry of the CD cavity, we used the circularity (*C*) calculated following Equation (3). The *C* values of all models at 300 K are listed in Table 3.  $\beta$ CD had the lowest *C* ( $0.727 \pm 0.087$ ), indicating that its conformational change is higher than those of other models. Moreover, the *C* values of Tet2Tet6-HP $\beta$ CDs are also very low ( $0.742 \pm 0.080$ ). The reason for this more flexible conformation may be the result from the higher steric hindrance of HP groups on both the O2 and O6 positions of the glucose subunits. In addition, taking the standard deviation into account, the *C* values of Tri6- and Tet6-HP $\beta$ CDs were found to be  $0.814 \pm 0.075$  and  $0.815 \pm 0.076$ , respectively. The data suggests that the cavity becomes more circular in shape, when increasing the number of substituting the HP at the O6 primary hydroxyl groups of up to three or four residues, corresponding to a high population of no-flip conformations. Although the population of no-flip conformations of Tri6-, Tet6- and Mon2Tet6-HP $\beta$ CDs, as well as that of Di2Tet6-HP $\beta$ CD, are quite similar (higher than 75%), the *C* values of Mon2Tet6- and Di2Tet6-HP $\beta$ CDs are lower than the Tri6- and Tet6-HP $\beta$ CDs, due to the steric hindrance of the HP groups, leading to a distortion of some glucose subunits in the no-flip conformation. For that reason, Tri6- and Tet6-HP $\beta$ CDs are highlighted as proper structures for forming inclusion complexes with guest molecules, as indicated from their high circularities with a lower possibility of flipping.

**Table 3.** The average and standard deviation of the circularity (*C*) of  $\beta$ CD and HP $\beta$ CDs at 300 K, using REMD simulations.

Models	<i>C</i>
$\beta$ CD	$0.727 \pm 0.087$
<b>Single-sided HP-substitution</b>	
Mon6-HP $\beta$ CD	$0.746 \pm 0.085$
Di6-HP $\beta$ CD	$0.751 \pm 0.086$
Tri6-HP $\beta$ CD	$0.814 \pm 0.075$
Tet6-HP $\beta$ CD	$0.815 \pm 0.076$
Hep6-HP $\beta$ CD	$0.773 \pm 0.088$
<b>Double-sided HP-substitution</b>	
Mon2Tet6-HP $\beta$ CD	$0.803 \pm 0.075$
Di2Tet6-HP $\beta$ CD	$0.767 \pm 0.076$
Tri2Tet6-HP $\beta$ CD	$0.785 \pm 0.074$
Tet2Tet6-HP $\beta$ CD	$0.742 \pm 0.080$

### 3.2. Cavity Self-Closure

The arrangement of the HP groups during simulations influences the CD cavity accessibility directly. Some HP groups can point toward the CD interior, leading to self-closure of the CD cavity. The arrangements of the HP substituents at the glucose subunits were monitored via the distance of the center of mass between the  $\beta$ CD ring and each HP group, called  $d_{4(i)}[C_{g(\beta CD)}-C_{g(HP(i))}]$ . The arrangement of HP for Mon6-HP $\beta$ CD is plotted in Figure 7, while those of the other HP $\beta$ CDs are shown in Figure S2.

During the REMD simulation of Mon6-HP $\beta$ CD, almost 98% of HP groups pointed toward the CD exterior, with  $d_{4(i)}[C_{g(\beta CD)}-C_{g(HP(i))}]$  around 7–10 Å. For Mon6-HP $\beta$ CD with  $d_{4(i)}[C_{g(\beta CD)}-C_{g(HP(i))}]$  in the rank from 7 to 12 Å, the shape of Mon6-HP $\beta$ CD seemed to be like a bowl (Figure 7a). When the  $d_{4(i)}[C_{g(\beta CD)}-C_{g(HP(i))}]$  was less than 3 Å, the HP group was hindered and rotated into the cavity of the  $\beta$ CD ring, leading to self-closure of the CD cavity (Figure 7c). We also found that the cavity self-closure was related to flipping of the HP-substituted glucose subunits, which triggers HP entrance into the CD cavity ( $d_{4(i)}[C_{g(\beta CD)}-C_{g(HP(i))}] \sim 1$  Å). Some snapshots show that the substituents enter the cavity at the narrow rim with  $d_{4(i)}[C_{g(\beta CD)}-C_{g(HP(i))}] \sim 2$  Å. For that reason, we defined the self-closure of CD cavity or HP occupied in the CD cavity when  $d_{4(i)}[C_{g(\beta CD)}-C_{g(HP(i))}] < 3$  Å. The numbers of

$d_{4(i)}[C_{g(\beta CD)}-C_{g(HP(i))}] < 3 \text{ \AA}$  were called  $n(HP_{\text{inserted}})$ , as illustrated in Equation (4). For all REMD simulations of HP $\beta$ CDs at 300 K,  $n(HP_{\text{inserted}})$  are plotted in Figure 8 with the probability in terms of the percentage of 25,000 snapshots. The results at the various temperatures are summarized in Table S2.

$$n(HP_{\text{inserted}}) = n(d_{4(i)}[C_{g(\beta CD)}-C_{g(HP(i))}] < 3 \text{ \AA}) \quad (4)$$

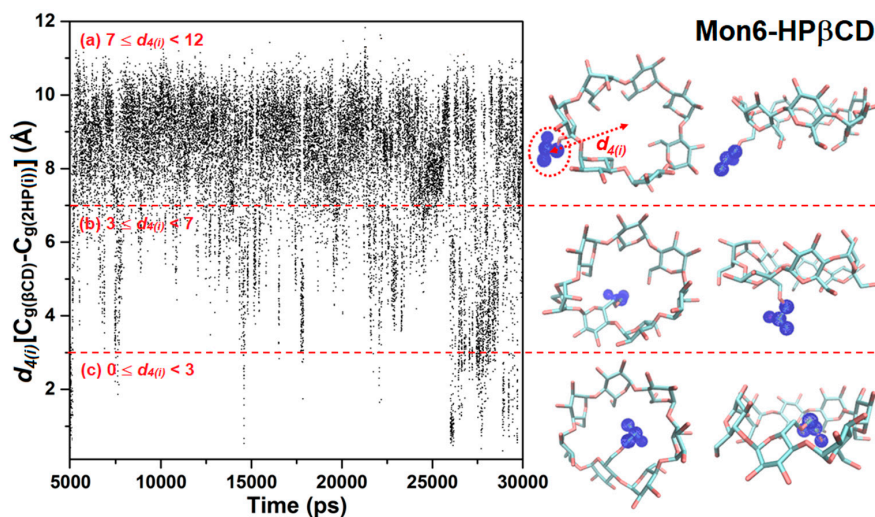


Figure 7. The distance of the centers of mass between the  $\beta$ CD ring and HP group,  $d_{4(i)}[C_{g(\beta CD)}-C_{g(HP(i))}]$  for Mon6-HP $\beta$ CD at 300 K.

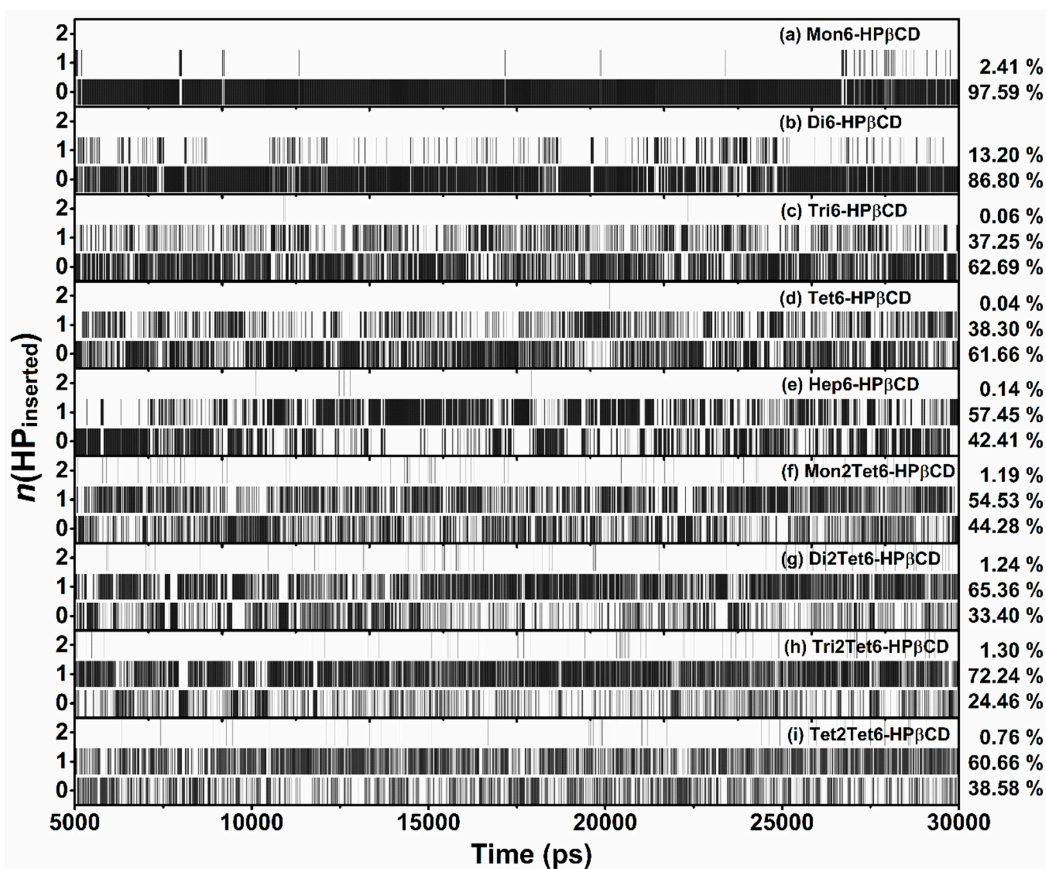
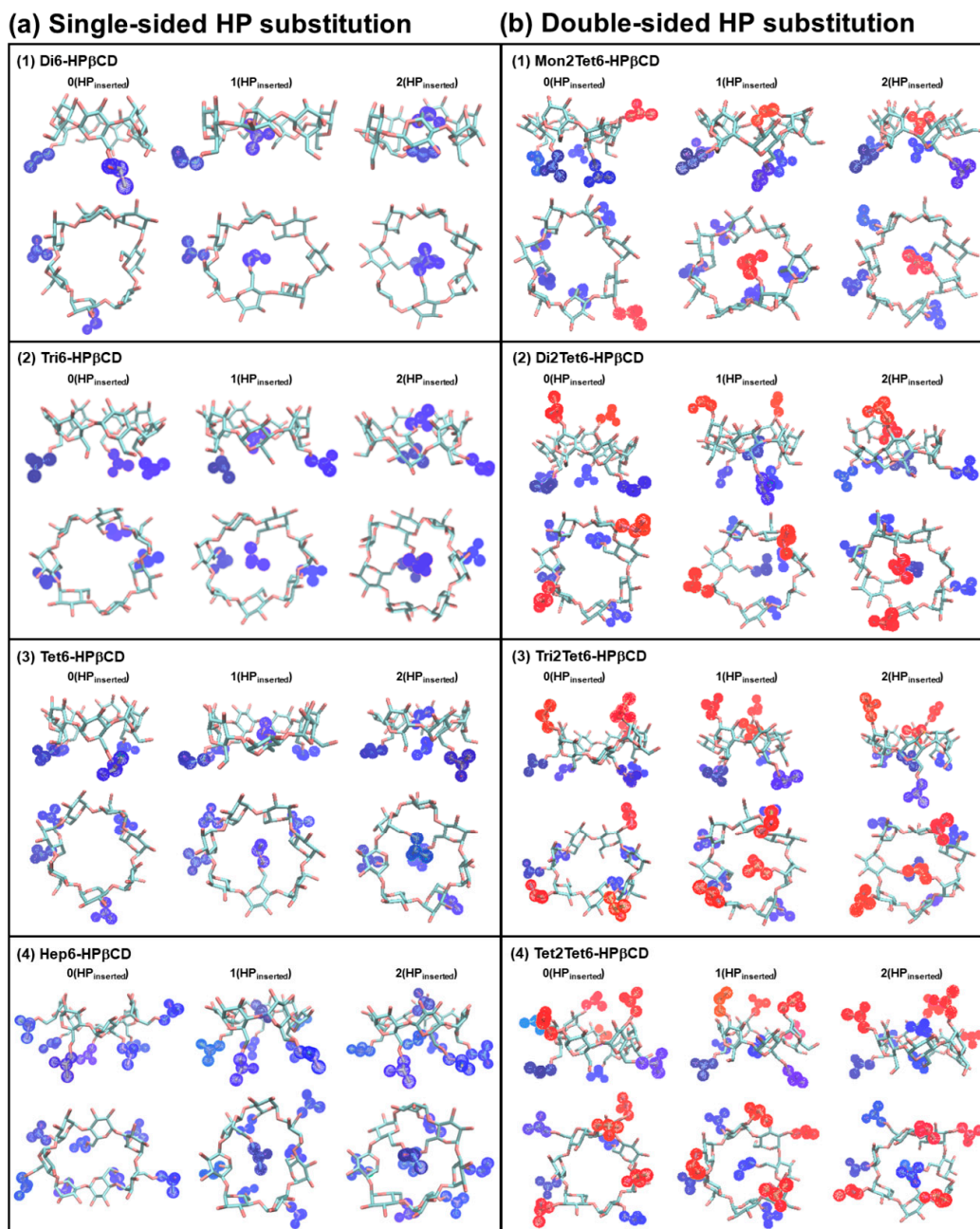


Figure 8. The probability of  $n(HP_{\text{inserted}})$  from 25,000 snapshots (criteria:  $d_{4(i)}[C_{g(\beta CD)}-C_{g(HP(i))}] < 3 \text{ \AA}$ ) at 300 K for all HP $\beta$ CDs.

For HP $\beta$ CDs with single-sided HP-substitutions, it was noticeable that when  $n(\text{HP}_{\text{inserted}}) > 0$ , the cavity self-closure occurred. Example snapshots of HP $\beta$ CDs with different numbers of  $n(\text{HP}_{\text{inserted}})$  are given in Figure 9. As shown in the figure, the flipped HP-substituted glucopyranose subunits and the HP groups inserted into the hydrophobic cavity led to cavity self-closure in the HP $\beta$ CDs. When the number of HP groups was increased, the percentage of cavity self-closure significantly increased from 2.41 to 57.59% in Hep6-HP $\beta$ CD. This indicates that the cavity of the HP $\beta$ CD structure was almost blocked when the number of HP-substitutions was increased. Furthermore, the maximum of  $n(\text{HP}_{\text{inserted}})$  was equal to 2, even in the HP $\beta$ CD with a high degree of HP-substitutions, such as Hep6-HP $\beta$ CD and Tet2Tet6-HP $\beta$ CD.



**Figure 9.** Example snapshots of different numbers of HP occupied in the CD cavity (criteria:  $d_{4(i)}[\text{C}_{\text{g}}(\beta\text{CD})-\text{C}_{\text{g}}(\text{HP}(i))] < 3 \text{ \AA}$ ) for all HP $\beta$ CDs at 300 K.

For HP $\beta$ CDs with double-sided HP-substitutions, the HP groups, both on the narrow and wider rim of HP $\beta$ CD could point into the cavity. For that reason, the percentage of cavity self-closure was higher than those of single-sided HP-substitutions, because of the large fluctuation of their structures. When increasing the number of HP groups at the O2 positions on Tet6-HP $\beta$ CD from one to four, the probability of cavity self-closure rose dramatically from 38.34% (Tet6-HP $\beta$ CD) to 55.72, 66.60, 73.54, and 61.42% for Mon2Tet6-, Di2Tet6-, Tri2Tet6-, and Tet2Tet6-HP $\beta$ CDs, respectively. With increasing temperatures, the glucose subunits distorted, and the HP groups fluctuated far from the center of mass of the  $\beta$ CD ring, leading to a lower probability of cavity self-closure at higher temperatures for all models (Table S2).

In summary, all data showed that the HP-substitution strongly affects the cavity self-closure of HP $\beta$ CD, especially when the number of the HP substituents increases. To prevent cavity self-closure, which might block the inclusion of the guest molecules, we suggest that the HP-substitution should be a single-sided substitution, with the degree of substitution being less than 0.57 such as Di-, Tri-, and Tet6-HP $\beta$ CDs. However, it should be mentioned that the above results were only valid in cases where there was no interaction between the cyclodextrins (at higher concentrations). Moreover, the change of the dielectric properties, e.g., by using solvent mixtures, might influence the conformations of the considered molecules, as well as their conformational equilibria.

#### 4. Conclusions

REMD simulations have been performed on HP $\beta$ CDs with various degrees of substitution (DS = 0.14–1.14) to study the structural behaviors and the effects of HP substituents. Several parameters that influence such changes have been identified. The circularity and the radius of gyration explain the size and shape of the cavity of the ring, and the flip angle and important distances describe the conformational changes and the flexibilities of the HP groups. The results show that HP $\beta$ CDs have a more pronounced conical shape than  $\beta$ CD; however, cavity self-closure occurs because some glucopyranoses with HP groups flip or distort, followed by one or two HP groups coming close to the CD cavity, thus hindering drug inclusion. HP $\beta$ CDs with high DS are more likely to be blocked, while HP $\beta$ CDs with double-sided HP-substitutions are even more likely to be blocked. Among the nine HP $\beta$ CDs, all analysis parameters point out that Tri- and Tet6-HP $\beta$ CDs with three and four HP-substitutions on the primary rim have a distinctive conformation, being mostly circular with a low possibility of flipping and cavity enclosure. Thus, these HP $\beta$ CDs could serve as more proper hosts for the encapsulation of low-water soluble compounds.

**Supplementary Materials:** The following are available online at <http://www.mdpi.com/2073-4360/11/1/145/s1>, Figure S1: The overlapping between the potential energy distributions of each replica temperature, ranging from 269.5 K to 570.9 K. Figure S2: The distance of the centers of mass between the  $\beta$ CD ring and the HP group,  $d_{4(i)}[C_{g(\beta CD)}-C_{g(HP(i))}]$  for (a) Di6-HP $\beta$ CD, (b) Tri6-HP $\beta$ CD, (c) Tet6-HP $\beta$ CD, (d) Hep6-HP $\beta$ CD, (e) Mon2Tet6-HP $\beta$ CD, (f) Di2Tet6-HP $\beta$ CD, (g) Tri2Tet6-HP $\beta$ CD, and (h) Tet2Tet6-HP $\beta$ CD at 300 K. Figures S3–S12: Contour graphs of the native  $\beta$ CD (S3), Mon6-HP $\beta$ CD (S4), Di6-HP $\beta$ CD (S5), Tri6-HP $\beta$ CD (S6), Tet6-HP $\beta$ CD (S7), Hep6-HP $\beta$ CD (S8), Mon2Tet6-HP $\beta$ CD (S9), Di2Tet6-HP $\beta$ CD (S10), Tri2Tet6-HP $\beta$ CD (S11), and Tet2Tet6-HP $\beta$ CD (S12), probability distributions of 25,000 snapshots with the glycam06 force field at various temperatures. Figure S13: The radius of gyration at various temperatures for (a)  $\beta$ CD, (b) Mon6-HP $\beta$ CD, (c) Di6-HP $\beta$ CD, (d) Tri6-HP $\beta$ CD, (e) Tet6-HP $\beta$ CD, (f) Hep6-HP $\beta$ CD, (g) Mon2Tet6-HP $\beta$ CD, (h) Di2Tet6-HP $\beta$ CD, (i) Tri2Tet6-HP $\beta$ CD, and (j) Tet2Tet6-HP $\beta$ CD. Table S1: The probabilities of different numbers of flip glucose subunits in  $\beta$ CD and all HP $\beta$ CDs, using the flip angle parameter,  $\theta_{(i)}[C_{6(i)}-C_{2(i+1)}-C_{6(i+1)}]$  at various temperatures (criteria: a value higher than 90 degree) compared with the classical MD simulation in the parenthesis. Table S2: The probability of the overall snapshots with different numbers of HP occupied in the CD cavity (criteria:  $d_{4(i)}[C_{g(\beta CD)}-C_{g(HP(i))}] < 3 \text{ \AA}$ ) for all HP $\beta$ CDs at various temperatures.

**Author Contributions:** K.K. analyzed all data and wrote the original draft. Some results of the classical MD simulation were analyzed by J.K., T.R. and N.K. conceived the conceptualization. P.W., S.M., C.R., M.K., H.O., N.K., and T.R. supervised the project. All authors discussed the results and contributed to the final manuscript.



**Acknowledgments:** T.R. and N.K. gratefully acknowledge the financial support from the Thailand Research Fund (RSA5980069 to T.R. and RSA6180044 to N.K.). This work was supported by a Grant-in-Aid for Scientific Research on Innovative Areas in “Precisely Designed Catalysts with Customized Scaffolding” (JSPS KAKENHI Grant Number JP18H04233 to S.M.). This research work was partially supported by Chiang Mai University. K.K. thanks W. Khuntawee, C. Hanpiboon, B. Nutho, and T. Saelee for resolving some technical problems. P.W. thanks Chulalongkorn University (CU) for a short-term visit grant. Travel grants for research visits, and for the research reported in this publication, were also supported by the ASEAN-European Academic University Network (ASEA-UNINET). The Center of Excellence Computational Chemistry (CU), and the Vienna Scientific Cluster (VSC-2) are gratefully thanked for providing computational facilities.

**Conflicts of Interest:** The authors declare no conflict of interest.

## References

1. Uekama, K.; Hirayama, F.; Irie, T. Cyclodextrin Drug Carrier Systems. *Chem. Rev.* **1998**, *98*, 2045–2076. [[CrossRef](#)] [[PubMed](#)]
2. Hirayama, F.; Uekama, K. Cyclodextrin-based controlled drug release system. *Adv. Drug Deliv. Rev.* **1999**, *36*, 125–141. [[CrossRef](#)]
3. Aachmann, F.L.; Otzen, D.E.; Larsen, K.L.; Wimmer, R. Structural background of cyclodextrin-protein interactions. *Protein Eng.* **2003**, *16*, 905–912. [[CrossRef](#)] [[PubMed](#)]
4. Davis, M.E.; Brewster, M.E. Cyclodextrin-based pharmaceuticals: Past, present and future. *Nat. Rev. Drug Discov.* **2004**, *3*, 1023–1035. [[CrossRef](#)] [[PubMed](#)]
5. Challa, R.; Ahuja, A.; Ali, J.; Khar, R.K. Cyclodextrins in drug delivery: An updated review. *AAPS PharmSciTech* **2005**, *6*, E329–E357. [[CrossRef](#)] [[PubMed](#)]
6. Loftsson, T.; Jarho, P.; Másson, M.; Järvinen, T. Cyclodextrins in drug delivery. *Expert Opin. Drug Deliv.* **2005**, *2*, 335–351. [[CrossRef](#)] [[PubMed](#)]
7. Brewster, M.E.; Loftsson, T. Cyclodextrins as pharmaceutical solubilizers. *Adv. Drug Deliv. Rev.* **2007**, *59*, 645–666. [[CrossRef](#)]
8. Marques, H.M.C. A review on cyclodextrin encapsulation of essential oils and volatiles. *Flavour Frag. J.* **2010**, *25*, 313–326. [[CrossRef](#)]
9. Crini, G. Review: A History of Cyclodextrins. *Chem. Rev.* **2014**, *114*, 10940–10975. [[CrossRef](#)] [[PubMed](#)]
10. Gould, S.; Scott, R.C. 2-Hydroxypropyl- $\beta$ -cyclodextrin (HP- $\beta$ -CD): A toxicology review. *Food Chem. Toxicol.* **2005**, *43*, 1451–1459. [[CrossRef](#)] [[PubMed](#)]
11. Schönbeck, C.; Westh, P.; Madsen, J.C.; Larsen, K.L.; Städe, L.W.; Holm, R. Hydroxypropyl-Substituted  $\beta$ -Cyclodextrins: Influence of Degree of Substitution on the Thermodynamics of Complexation with Tauroconjugated and Glycoconjugated Bile Salts. *Langmuir* **2010**, *26*, 17949–17957. [[CrossRef](#)] [[PubMed](#)]
12. Reyes-Reyes, M.L.; Roa-Morales, G.; Melgar-Fernández, R.; Reyes-Pérez, H.; Gómez-Oliván, L.; Gonzalez-Rivas, N.; Bautista-Renedo, J.; Balderas-Hernández, P. Chiral recognition of abacavir enantiomers by (2-hydroxy)propyl- $\beta$ -cyclodextrin: UHPLC, NMR and DFT studies. *J. Incl. Phenom. Macrocycl. Chem.* **2015**, *82*, 373–382. [[CrossRef](#)]
13. Yuan, C.; Liu, B.; Liu, H. Characterization of hydroxypropyl- $\beta$ -cyclodextrins with different substitution patterns via FTIR, GC-MS, and TG-DTA. *Carbohydr. Polym.* **2015**, *118*, 36–40. [[CrossRef](#)] [[PubMed](#)]
14. Buvári-Barcza, Á.; Barcza, L. Influence of the guests, the type and degree of substitution on inclusion complex formation of substituted  $\beta$ -cyclodextrins. *Talanta* **1999**, *49*, 577–585. [[CrossRef](#)]
15. Yuan, C.; Jin, Z.; Li, X. Evaluation of complex forming ability of hydroxypropyl- $\beta$ -cyclodextrins. *Food Chem.* **2008**, *106*, 50–55. [[CrossRef](#)]
16. Concha-Santos, S.; Pérez-Casas, S.; Brocos, P.; Piñeiro, Á. Testing the effect of the cavity size and the number of molecular substitutions in host-guest complexes formed by 2-hydroxypropyl-cyclodextrins and n-octyl- $\beta$ -D-glucopyranoside. *J. Chem. Thermodyn.* **2013**, *67*, 112–119. [[CrossRef](#)]
17. Yong, C.; Washington, C.; Smith, W. Structural Behaviour of 2-Hydroxypropyl- $\beta$ -Cyclodextrin in Water: Molecular Dynamics Simulation Studies. *Pharm. Res.* **2008**, *25*, 1092–1099. [[CrossRef](#)] [[PubMed](#)]



18. Pitha, J.; Trinadha Rao, C.; Lindberg, B.; Seffers, P. Distribution of substituents in 2-hydroxypropyl ethers of cyclomaltoheptaose. *Carbohydr. Res.* **1990**, *200*, 429–435. [[CrossRef](#)]
19. Trinadha Rao, C.; Pitha, J.; Lindberg, B.; Lindberg, J. Distribution of substituents in O-(2-hydroxypropyl) derivatives of cyclomalto-oligosaccharides (cyclodextrins): Influence of increasing substitution, of the base used in the preparation, and of macrocyclic size. *Carbohydr. Res.* **1992**, *223*, 99–107. [[CrossRef](#)]
20. Buvári-Barcza, Á.; Bodnár-Gyarmathy, D.; Barcza, L. Hydroxypropyl- $\beta$ -cyclodextrins: Correlation between the stability of their inclusion complexes with phenolphthalein and the degree of substitution. *J. Incl. Phenom. Mol. Recognit. Chem.* **1994**, *18*, 301–306. [[CrossRef](#)]
21. Malanga, M.; Szemán, J.; Fenyvesi, É.; Puskás, I.; Csabai, K.; Gyémánt, G.; Fenyvesi, F.; Szente, L. “Back to the Future”: A New Look at Hydroxypropyl Beta-Cyclodextrins. *J. Pharm. Sci.* **2016**, *105*, 2921–2931. [[CrossRef](#)] [[PubMed](#)]
22. Nutho, B.; Nunthaboot, N.; Wolschann, P.; Kungwan, N.; Rungrotmongkol, T. Metadynamics supports molecular dynamics simulation-based binding affinities of eucalyptol and beta-cyclodextrin inclusion complexes. *RSC Adv.* **2017**, *7*, 50899–50911. [[CrossRef](#)]
23. Sugita, Y.; Okamoto, Y. Replica-exchange molecular dynamics method for protein folding. *Chem. Phys. Lett.* **1999**, *314*, 141–151. [[CrossRef](#)]
24. Hukushima, K.; Nemoto, K. Exchange Monte Carlo Method and Application to Spin Glass Simulations. *J. Phys. Soc. Jpn.* **1996**, *65*, 1604–1608. [[CrossRef](#)]
25. Hansmann, U.H.E. Parallel tempering algorithm for conformational studies of biological molecules. *Chem. Phys. Lett.* **1997**, *281*, 140–150. [[CrossRef](#)]
26. Nymeyer, H.; Gnanakaran, S.; García, A.E. Atomic Simulations of Protein Folding, Using the Replica Exchange Algorithm. In *Methods in Enzymology*; Academic Press: Cambridge, MA, USA, 2004; Volume 383, pp. 119–149.
27. Cheng, X.; Cui, G.; Hornak, V.; Simmerling, C. Modified Replica Exchange Simulation Methods for Local Structure Refinement. *J. Phys. Chem. B* **2005**, *109*, 8220–8230. [[CrossRef](#)] [[PubMed](#)]
28. Snor, W.; Liedl, E.; Weiss-Greiler, P.; Karpfen, A.; Viernstein, H.; Wolschann, P. On the structure of anhydrous  $\beta$ -cyclodextrin. *Chem. Phys. Lett.* **2007**, *441*, 159–162. [[CrossRef](#)]
29. Kicuntod, J.; Khuntawee, W.; Wolschann, P.; Pongsawasdi, P.; Chavasiri, W.; Kungwan, N.; Rungrotmongkol, T. Inclusion complexation of pinostrobin with various cyclodextrin derivatives. *J. Mol. Graph. Model.* **2016**, *63*, 91–98. [[CrossRef](#)] [[PubMed](#)]
30. Case, D.A.; Babin, V.; Berryman, J.T.; Betz, R.M.; Cai, Q.; Cerutti, D.S.; Cheatham, T.E.; Darden, T.A.; Duke, R.E.; Gohlke, H.; et al. *AMBER 14*; University of California, San Francisco: San Francisco, CA, USA, 2014.
31. Kirschner, K.N.; Yongye, A.B.; Tschampel, S.M.; González-Outeiriño, J.; Daniels, C.R.; Foley, B.L.; Woods, R.J. GLYCAM06: A generalizable biomolecular force field. *Carbohydrates. J. Comput. Chem.* **2008**, *29*, 622–655. [[CrossRef](#)]
32. Tessier, M.B.; DeMarco, M.L.; Yongye, A.B.; Woods, R.J. Extension of the GLYCAM06 biomolecular force field to lipids, lipid bilayers and glycolipids. *Mol. Simul.* **2008**, *34*, 349–364. [[CrossRef](#)]
33. Khuntawee, W.; Rungrotmongkol, T.; Wolschann, P.; Pongsawasdi, P.; Kungwan, N.; Okumura, H.; Hannongbua, S. Conformation study of  $\epsilon$ -cyclodextrin: Replica exchange molecular dynamics simulations. *Carbohydr. Polym.* **2016**, *141*, 99–105. [[CrossRef](#)]
34. Khuntawee, W.; Kunaseth, M.; Rungnim, C.; Intagorn, S.; Wolschann, P.; Kungwan, N.; Rungrotmongkol, T.; Hannongbua, S. Comparison of Implicit and Explicit Solvation Models for Iota-Cyclodextrin Conformation Analysis from Replica Exchange Molecular Dynamics. *J. Chem. Inf. Model.* **2017**, *57*, 778–786. [[CrossRef](#)] [[PubMed](#)]
35. Wongpituk, P.; Nutho, B.; Panman, W.; Kungwan, N.; Wolschann, P.; Rungrotmongkol, T.; Nunthaboot, N. Structural dynamics and binding free energy of neral-cyclodextrins inclusion complexes: Molecular dynamics simulation. *Mol. Simul.* **2017**, *43*, 1356–1363. [[CrossRef](#)]

36. Mahalapbutr, P.; Nutho, B.; Wolschann, P.; Chavasiri, W.; Kungwan, N.; Rungrotmongkol, T. Molecular insights into inclusion complexes of mansonone E and H enantiomers with various  $\beta$ -cyclodextrins. *J. Mol. Graph. Model.* **2018**, *79*, 72–80. [[CrossRef](#)] [[PubMed](#)]
37. Mahalapbutr, P.; Thitinthavet, K.; Kedkham, T.; Nguyen, H.; thi ha Theu, L.; Dokmaisrijan, S.; Huynh, L.; Kungwan, N.; Rungrotmongkol, T. A theoretical study on the molecular encapsulation of luteolin and pinocembrin with various derivatized beta-cyclodextrins. *J. Mol. Struct.* **2018**, in press. [[CrossRef](#)]



© 2019 by the authors. Licensee MDPI, Basel, Switzerland. This article is an open access article distributed under the terms and conditions of the Creative Commons Attribution (CC BY) license (<http://creativecommons.org/licenses/by/4.0/>).